Studies on Melt-Spinning Process of Hollow Fibers

TAE HWAN OH,[1] MOO SEOK LEE,[1] SANG YONG KIM,[1] HYUN JOO SHIM[2]

[1] Department of Fiber and Polymer Science, College of Engineering, Seoul National University, San 56-1, Shinlim-Dong, Kwanak-Ku, Seoul 151-742, South Korea

[2] Department of Textile Engineering, Soongsil University, Seoul, South Korea

Received 30 May 1997; accepted 3 September 1997

ABSTRACT: Profile development and dimensional change in the melt-spinning process of hollow fibers were studied using a finite element method, and a numerical simulation was compared with experimental results. The numerical simulation of a hollow-fiber spinning process was carried out by considering the changes in inner and outer boundaries. Initial dimensions of inner and outer radii were obtained by measuring the dimensions of extrudate at the extrudate swell point using a capturing device. Extrudate swell plays an important role in determining the initial dimensions of the inner and outer radii, but has less effect on the hollow portion at the die swell point. The effects of spinning variables on the hollow portion show that spinning temperature is the most critical variable in controlling the hollow portion, followed by mass throughput rate. Take-up velocity has relatively less effect. As the mass throughput rate and take-up velocity increase and the spinning temperature decreases, the hollow portion of as-spun fiber increases. © 1998 John Wiley & Sons, Inc. J Appl Polym Sci 68: 1209–1217, 1998

Key words: hollow fiber; finite element method; numerical simulation; hollow portion; extrudate swell

INTRODUCTION

There has been great development in the methodology to manufacture shaped fibers which have a noncircular cross section similar to die geometry.[1,2] A noncircular cross-sectional shape of fibers shows properties different from cylindrical fibers with a circular cross section, in bending stiffness, coefficient of friction, softness, and handle.[3] Hollow fiber is a kind of shaped fiber and there are two types of a spinneret design that manufacture it. One type uses an annular die with a system of air blowing into the inner core to form a hollow portion,[4] and the other uses a segmented arc-type die which induces an inflow of air.[5,6] Inflow of air between segmented arcs in the latter serves as blowing of air into the inner core of the former.

There has been much progress in the analysis of the melt-spinning process. Ziabicki[7] has developed a fundamental theoretical understanding of the melt-spinning process. Kase and Matsuo[8,9] generalized a numerical analysis of the melt-spinning process: their work was done by solving the thin-filament equations, which were formulated by averaging the sets of fundamental governing equations over the cross section of running filament with the appropriate empirical relations for physical properties and the transport coefficients. After their work, theoretical process analyses have been extended and developed by many others.[10–12]

The difference between the spinning process of hollow fiber and that of cylindrical fiber is due to

Correspondence to: T. H. Oh.

Contract grant sponsor: Research Fund for Advanced Materials, Ministry of Education, Republic of Korea (1996).

Journal of Applied Polymer Science, Vol. 68, 1209–1217 (1998)
 CCC 0021-8995/98/081209-09

an additional dimensional variable (inner radius), and thus another consideration about inner boundary is needed. Freeman and colleagues[4] and Getmanyuk and associates[13] studied the isothermal drawing of hollow tubes and the dynamics of the spinning process of polycarbonatesiloxane hollow fiber.

Finite element method has been generally used to study a flow in the upstream region and the extrudate swell of fluid emerging from a die.[14–16] Because a spinline has a very large length-to-diameter ratio (L/D) and a large drawdown ratio, and because some boundary conditions have to be satisfied, an application of the finite element method to the whole spinline has not been done effectively.

In the case of hollow-fiber spinning, an application of an asymptotic method (such as the thin-filament equations used in the analysis of a melt-spinning process) is not convenient because of the additional variable; thus a two-dimensional finite element method which generates the inner and outer boundaries can be applied.

In this work, the dynamics of a hollow-fiber spinning process was simulated using a finite element method, and the die-swell characteristics were observed to obtain initial dimensions. Also, the changes in final dimensions were determined and the simulation of the effect of spinning variables on the process was compared with the experiment.

FORMULATION AND NUMERICAL METHOD

A cylindrical coordinate system was employed and the velocity for θ direction was neglected in the formulation.

For steady flow, the equations for conservation of mass and momentum are as follows:

$$\nabla \cdot \mathbf{v} = 0 \tag{1}$$

$$\rho \mathbf{v} \cdot \nabla \mathbf{v} = \rho \mathbf{f} + \nabla \cdot \sigma = -\nabla p + \rho \mathbf{f} + \nabla \cdot \tau \tag{2}$$

where $\mathbf{v}$ represents the velocity vector, ρ the density, $\mathbf{f}$ the body force, σ the total stress tensor, p the pressure, and τ the deviatoric stress tensor.

The velocity vector can be written as follows:

$$\mathbf{v} = [v_r(r, z), 0, v_z(r, z)] \tag{3}$$

where $v_r(r, z)$ and $v_z(r, z)$ are the radial and axial velocity components, respectively.

Here, the fluid is assumed to be incompressible and Newtonian. The constitutive equation of Newtonian fluid is presented as

$$\tau = 2\eta \mathbf{D} \tag{4}$$

where $\mathbf{D}$ is the rate of strain tensor and η the Newtonian viscosity.

The viscosity of polymer is a function of temperature; the equation presented by Cao and coworkers[17] was used for this simulation.

$$\eta = 760 \exp\left(\frac{1670}{T + 273}\right) \quad T > 141°\text{C}$$

$$= 17.93 \exp\left(\frac{3190}{T + 273}\right) \quad 110°\text{C} < T < 141°\text{C} \tag{5}$$

where T is the temperature of polymer.

The $\mathbf{D}$ is presented as follows:

$$\mathbf{D} = \begin{pmatrix} \dfrac{\partial v_r}{\partial r} & 0 & \dfrac{1}{2}\left(\dfrac{\partial v_r}{\partial z} + \dfrac{\partial v_z}{\partial r}\right) \\ 0 & \dfrac{v_r}{r} & 0 \\ \dfrac{1}{2}\left(\dfrac{\partial v_r}{\partial z} + \dfrac{\partial v_z}{\partial r}\right) & 0 & \dfrac{\partial v_z}{\partial z} \end{pmatrix} \tag{6}$$

The transport of thermal energy in the fluid is described by

$$W_p C_p \frac{\partial T}{\partial z} = -\pi D_o h (T - T_\infty) \tag{7}$$

where W_p is the mass throughput rate, C_p the heat capacity, D_o the outer diameter of filament, h the heat transfer coefficient of the polymer, and T_∞ the temperature of surrounding air. To derive this equation, the temperature field is assumed to have no radial distribution. Both axial conduction and radial convection are neglected, and viscous dissipation is assumed to be negligible. A fourth-order Runge–Kutta method is utilized to solve the asymptotic energy equation, and this belongs to the finite element main code as a subroutine.

The axial temperature profile is obtained from this procedure.

The boundary and initial conditions for the velocity and for the temperature are as follows:

$$\left.\begin{aligned} &v_r(r, 0) = v_r(r, L) = 0 \\ &v_z(r, 0) = v_o \\ &v_z(r, L) = v_L \\ &T(0) = T_{\text{die}} \end{aligned}\right\} \tag{8}$$

where v_o is the initial velocity, v_L the final velocity (that is, take-up velocity), and T_{die} the spinning temperature. To generate the inner and outer moving boundaries on every iteration, no cross-flow condition is given at the inner and outer boundaries.

Several correlations for physical properties and the transport coefficients are expressed as[17]

$$\rho_p = 0.912 - (4.8 \times 10^{-4} T) \tag{9}$$

$$h = 0.42\left(\frac{k_a}{D_o}\right) Re_d^{0.334}\left[1 + \left(\frac{8v_a}{v_z}\right)^2\right]^{0.167} \tag{10}$$

$$\text{Re}_d = \left(\frac{v_z D_o}{\nu_a}\right) \tag{11}$$

where ρ_p is the density of the polymer, k_a the thermal conductivity of air, Re_d the Reynolds number, v_a the quench air velocity, v_z the velocity of filament, and ν_a the kinematic viscosity of air.

Equations (1), (2), (4), and (7) are the basic equations of finite element code used in this study. Since the finite element scheme has been described in detail elsewhere,[14,16] the derivation will not be presented but will be mentioned briefly here. The Galerkin formulation procedure was used to make a weak statement, and nonlinear forms of the above equations were solved using a Newton–Raphson iteration method. A nine-node rectangular element was used with 10 elements for the radial direction and 100 elements for the axial direction. Quadratic interpolation was used for the velocities and linear interpolation was used for the pressure.

The initial finite element grid is shown in Figure 1(a). Because of the rapid development of the profiles near the region of the spinneret, an unequal division of grid is required. In the neighboring region of the spinneret, the grid is finely formed; after the solidification point, it is divided broadly because changes of profile can hardly occur from the solidification point to take-up.

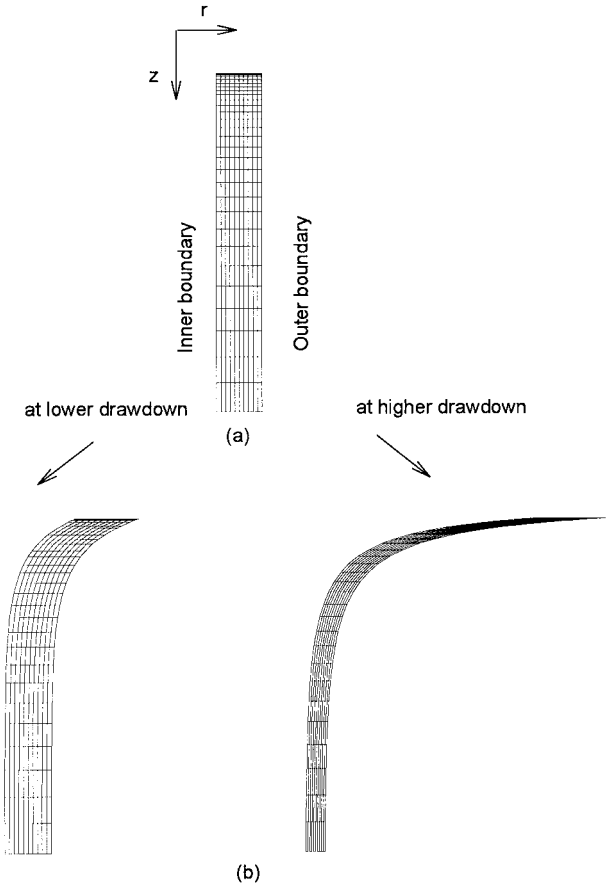

Figure 1 Finite element grid: (a) initial grid; (b) final grid.

EXPERIMENTAL

The die used in the experiment consists of a three-segmented arc, of which the outer radius was 0.05 cm and the inner radius 0.04 cm. The polymeric material was textile-grade isotactic polypropylene (PP) for which the number-average molecular weight was 36,900 and the weight-average molecular weight was 211,000. Spinning conditions used in this work are presented in Table I.

To obtain the radius profile, on-line measurement of radius along the spinline was carried out with a capturing device which can trap a running filament. As soon as the filament was captured, it was cooled to prevent loosening of the trapped molten extrudate. A high-resolution digital cam-

Table I Conditions Used in the Melt-Spinning of Hollow Fibers

Variables	Conditions
Mass throughput rate (g/min)	1.75, 2.0, 2.25, 2.5
Take-up speed (m/min)	50, 150, 250, 350
Spinning temperature (°C)	190, 210, 230, 250
Spin length (cm)	144

era was prepared on the spinline to confirm the dimensions of the captured object. Initial dimensions at a die swell point were measured from the captured extrudate. The captured running filament and as-spun fiber were carefully cut with a microtome to prepare the cross-section. An image analysis system with a built-in microscope was used to measure the inner and outer radii and cross-sectional area.

Percent ratio of hollow portion (A_i/A_t) is defined to represent the magnitude of hollow portion. Here, A_i denotes the cross-sectional area of the inner hollow part and A_t the total cross-sectional area.

RESULTS AND DISCUSSION

The numerical simulation was verified for accurate operation by solving a problem with a known exact solution. Verification was successfully performed within five iterations, and more than 20 iterations were needed for convergence in practical calculations. The grid was altered on every iteration until a convergence was achieved. The initial and final grids are shown in Figure 1. The grid dimension for the radial direction was greatly exaggerated so a deformation of the grid was clearly visible. A drastic change in the radius profile was observed below the spinneret but almost no change was observed near the solidification point.

Typical temperature and stress-profile developments of hollow fibers compared with those of cylindrical fibers are shown in Figure 2. If the same process conditions are defined, the rate of cooling and the stress along the spinline in hollow fibers are greater than those in cylindrical fibers and the length from spinneret to solidification point becomes shorter. Hollow fibers have a greater stress at a solidification point, which is due to rapid solidification, and this can lead to a superior tensile property of as-spun hollow fiber.[18]

Before simulation was carried out, initial values of inner and outer radii at the maximum extrudate swell point had to be determined. In the case of a cylindrical fiber-spinning process with a sufficient long spinline, little error would be introduced to a numerical simulation with die dimensions as initial conditions, i.e., die swell can be neglected. However, in the hollow fiber-spinning process, swollen initial dimensions are more important. For this purpose, as stated in the experiment, inner and outer radii at a die swell point were measured. Figure 3 shows the cross-section of captured extrudate at the die swell point [Fig. 3(a)] and that of as-spun fiber [Fig. 3(b)]. The cross-section at the die swell point deviates from a perfect circular shape because die swell at the center of the arc is greater than that at the edge. This is due to a difference of extrudate swell caused by the geometry of a segmented arc. The die of the segmented arc type has the die swell characteristic of an annular die at the center of the arc and that of a slit die at the edge of the arc. In the case of a slit die, flow is concentrated to the center because of higher shear rate at the center and low shear rate at the edge, giving a decrease of flow rate and leading to relatively low swell at the edge of the die.[19] The die swollen shape can affect the final cross-sectional shape of as-spun fiber because the molten extrudate will be deformed to a final shape maintaining an ini-

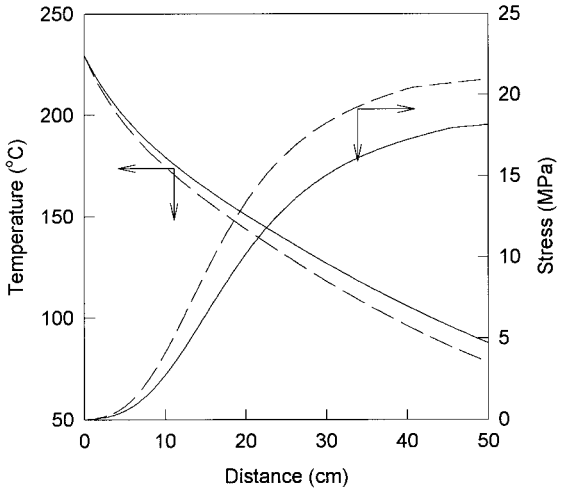

Figure 2 Comparison of computed temperature and stress profile along the spinline of hollow fiber with those of cylindrical fiber: (—) cylindrical fiber; (– – –) hollow fiber.

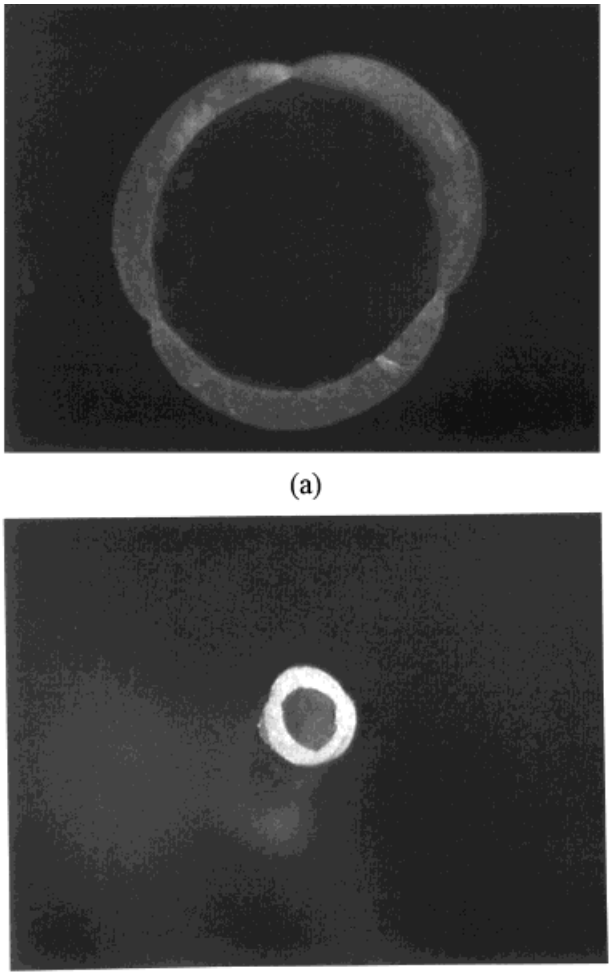

Figure 3 (caption to be inserted).

tial die swollen shape. Ziabicki[18] reported that the cross section of a shaped fiber on the spinline would be an intermediate shape between initial die shape and final shape.

Figures 4 through 6 show die swell characteristics with spinning parameters. Three types of swell ratio are the inner diameter swell ratio, χ_i; the outer diameter swell ratio, χ_o; and the thickness swell ratio, χ_t, defined as follows:

$$\chi_i = D_i^e/D_i^s \tag{12}$$

$$\chi_o = D_o^e/D_o^s \tag{13}$$

$$\chi_t = (D_o^e - D_i^e)/(D_o^s - D_i^s) \tag{14}$$

where D_i^e is the inner diameter at the maximum extrudate swell point, D_i^s the inner diameter at the spinneret, D_o^e the outer diameter at the maximum extrudate swell point, and D_o^s the outer diameter at the spinneret. The effect of mass throughput rate on extrudate swell is shown in Figure 4. It is shown that χ_i, χ_o, and χ_t are larger than unity, and this is reported in cases of both simulation[15] and experiment using an annular die.[20] The extrudate swell through a short channel can be explained by the relaxation and elastic recovery phenomena, and it depends on shear rate, molecular weight distribution, the L/D of channel, and the difference in diameter of the extrusion reservoir and orifice. Increasing a mass throughput rate results in increased shear rate of melt in the spinneret, and this causes an increase in melt elasticity and extrudate swell. As shown in Figure 4, χ_o is slightly larger than χ_i, and χ_t is larger than the both χ_i and χ_o. For the annular die, it is reported that χ_t is either equal to or slightly larger than χ_o; and in the case of PP, χ_t is larger than χ_o.[21] Thus it is seen that a die of the segmented arc type used in this work has a die swell characteristic similar to an annular die.

From Figure 5, it can be seen that χ_t decreases rapidly with the increase in spinning temperature, and both χ_i and χ_o decrease slowly with the spinning temperature. The relaxation time of polymer, which is related to melt elasticity, in-

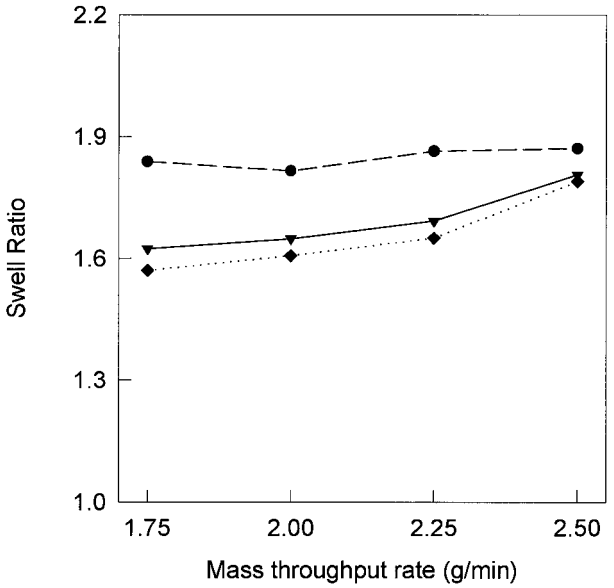

Figure 4 Die-swell ratio as a function of mass throughput rate: (●) thickness swell (χ_t); (▼) outer diameter swell (χ_o); (♦) inner diameter swell (χ_i).

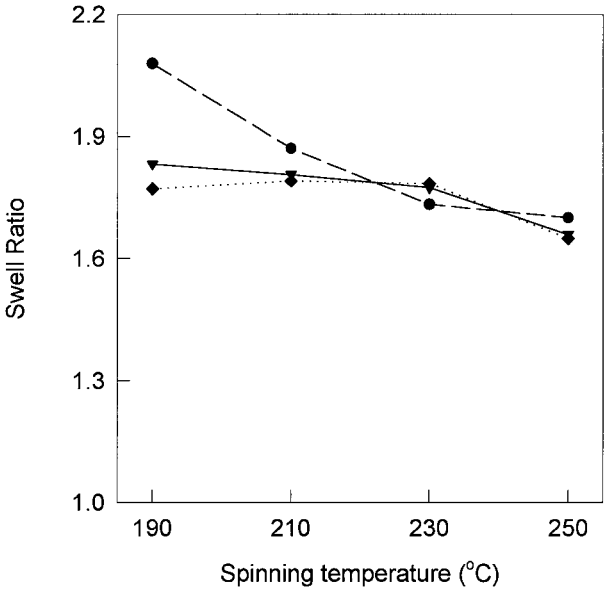

Figure 5 Die-swell ratio as a function of spinning temperature: (●) thickness swell (χ_t); (▼) outer diameter swell (χ_o); (♦) inner diameter swell (χ_i).

creases at the lower temperature and the extrudate swell increases. It is a general trend for polymers that the extrudate swell increases at lower melt temperature.[22] Die swell decreases slightly with increasing take-up velocity (Fig. 6). Swelling

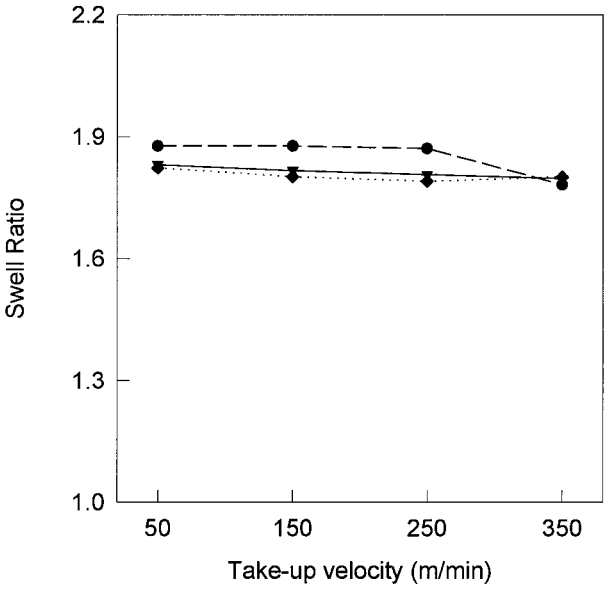

Figure 6 Die-swell ratio as a function of take-up velocity: (●) thickness swell (χ_t); (▼) outer diameter swell (χ_o); (♦) inner diameter swell (χ_i).

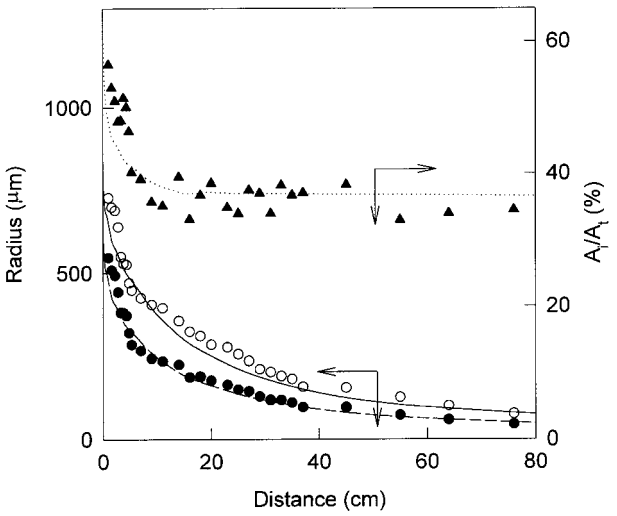

Figure 7 Radius profile and A_i/A_t profile. Inner radius: (●) experimental; (– – –) calculated. Outer radius: (○) experimental; (—) calculated. A_i/A_t: (▲) experimental; (· · · ·) calculated.

and drawing are interactive; and the high drawdown caused by increasing the take-up velocity results in an increased pulling force and reduces the die swell, but its effect is rather weak in this experiment.

As shown in Figures 4 through 7, die swell characteristics of inner and outer diameters are similar. The initial dimensions obtained from the results of the die swell were used for a numerical simulation. According to the results of die swell, initial dimensions vary with process variables, but little change occurs in the initial hollow portion at the die swell point compared with that at the die because of the increase of both the inner and outer diameters.

The magnitude of the hollow portion of as-spun fibers is an important factor and is a variable that can be controlled by changing mass throughput rate, spinning temperature, and take-up velocity. Instead of the inner-to-outer-radius ratio (R_i/R_o), the ratio A_i/A_t is commonly used to estimate the hollow portion of as-spun fibers because the cross-sectional shape may deviate from a perfect circular cross section.

Figure 7 shows the radius profile and the A_i/A_t profile under a typical spinning condition along the spinline. From the figure, it can be seen that the simulated radius profile stabilizes asymptotically and that experimental data coincides with simulation. The inner and outer radii are de-

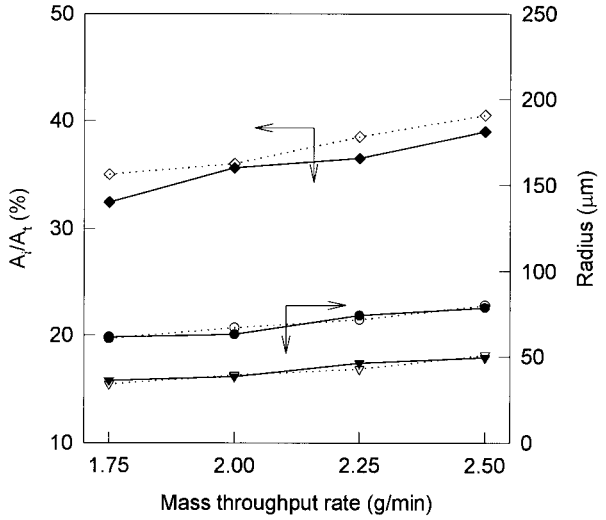

Figure 8 Radii and A_i/A_t of as-spun fiber as a function of mass throughput rate. Outer radius: (●) experimental; (○) calculated. Inner radius: (▼) experimental; (▽) calculated. A_i/A_t: (◆) experimental; (◇) calculated.

formed with a similar trend, and A_i/A_t decreases along the spinline and its value at the solidification point is much less than that at the die. Rapid reduction of A_i/A_t occurs at the initial deformation zone and stabilizes asymptotically to its final value.

The final dimensions of the inner and outer radii and A_i/A_t, including the experimental and simulated values, are shown in Figures 8 through 10. The A_i/A_t ratio of as-spun fiber is influenced by the change in the inner and outer radii. Effect of mass throughput rate on the final dimensions is shown in Figure 8. Increasing mass throughput rate at a constant take-up velocity makes fibers thick, and increase of both inner and outer radii causes an increase in A_i/A_t. The simulated data are quite consistent with the experimental data.

Figure 9 shows the effect of spinning temperature on A_i/A_t. Spinning temperature strongly affects A_i/A_t of as-spun fiber. The inner and outer radii of as-spun fiber increase with decreasing spinning temperature. This characteristic of hollow fiber differs from that of cylindrical fiber. In the case of the cylindrical fibers, if drawdown ratio (which is determined by mass throughput rate and take-up velocity) is fixed, little change will occur in the radius at the take-up point regardless of the change of spinning temperature, i.e., dimensions at the take-up point can be determined only by the drawdown ratio. On the other hand, the inner and outer radii of hollow fiber vary with spinning temperature; thus A_i/A_t becomes a function of spinning temperature. Though the cross-sectional area does not change under the same drawdown, A_i/A_t varies with the change in radii. This may be due to the fact that at a lower spinning temperature the fiber cools more quickly, and thus the deformation zone in the spinline becomes short and the inner and outer radii increase. In the case of the spinning temperature of 190°C, no increase in the hollow portion occurred in the experimental data.

Take-up velocity gives a change to the final dimensions but it has less effect on the change of A_i/A_t (Fig. 10). Increasing take-up velocity makes the fibers thin and the cross-sectional area and radii decrease. Though both inner and outer radii decrease, a decrease of the outer radius larger than that of the inner radius at a higher take-up velocity with a large drawdown causes the increase in A_i/A_t.

Figure 11 shows the sensitivity analysis of A_i/A_t at the die swell point and that of as-spun fiber to the changes of given spinning variables. It is shown that the most critical process variable changing the A_i/A_t ratio of as-spun fiber is the spinning temperature, followed by the mass throughput rate. The take-up velocity has a rel-

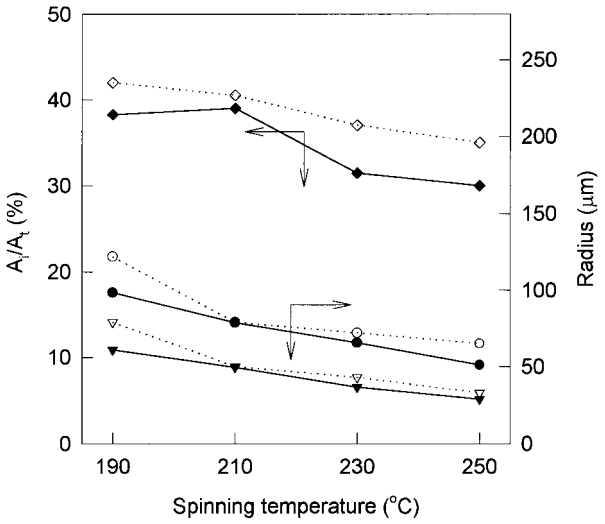

Figure 9 Radii and A_i/A_t of as-spun fiber as a function of spinning temperature. Outer radius: (●) experimental; (○) calculated. Inner radius: (▼) experimental; (▽) calculated. A_i/A_t: (◆) experimental; (◇) calculated.

atively lesser effect. Comparing the result at the extrudate swell point with that of as-spun fiber, little change is observed in A_i/A_t at the extrudate swell point. It is evident that die swell characteristics only slightly affect the hollow portion of as-spun fiber. Though the inner and outer radii are changed by extrudate swell, little change would occur in A_i/A_t at a die swell point, i.e., a deformation process along the spinline is dominant in the change of the hollow portion of as-spun fibers.

CONCLUSIONS

The dynamics of a melt-spinning process of hollow fibers can be described using a two-dimensional finite element method by considering the inner and outer moving boundaries. Die swell characteristics play an important role in determining the initial dimensions, but little change occurs in the hollow portion at the extrudate swell point as compared with that at the die. The deformation process along the spinline associated with spinning variables is the main factor controlling the hollow portion of as-spun fiber. Spinning temperature has a strong effect on the hollow portion of as-spun fiber, followed by mass throughput rate; take-up velocity has a lesser effect. Increasing the mass throughput rate and take-up velocity and lowering the spinning temperature lead to the increase in the hollow portion of as-spun fiber.

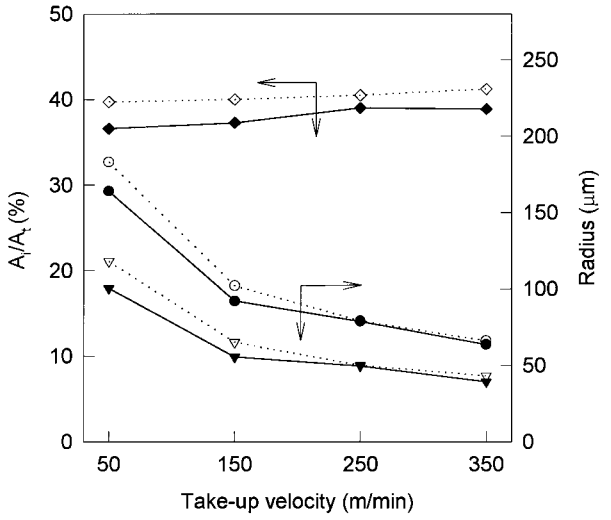

Figure 10 Radii and A_i/A_t of as-spun fiber as a function of take-up velocity. Outer radius: (●) experimental; (○) calculated. Inner radius: (▼) experimental; (▽) calculated. A_i/A_t: (♦) experimental; (◇) calculated.

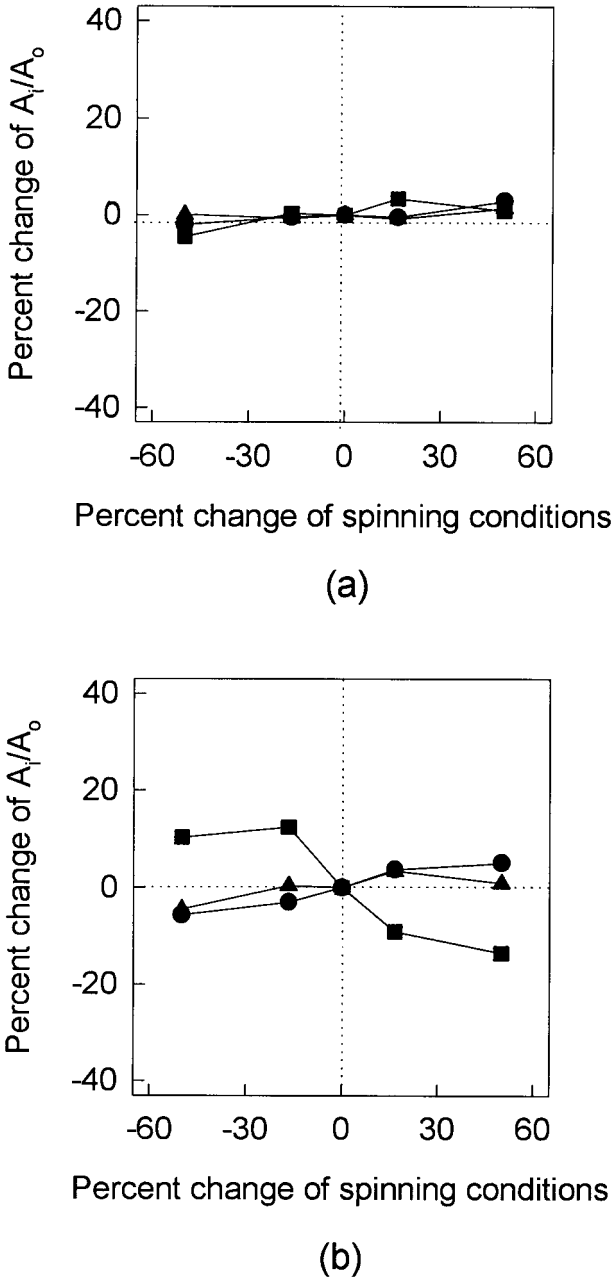

Figure 11 Sensitivity analysis of A_i/A_t for different spinning conditions: (a) at extrudate swell point; (b) as-spun fiber. (●) mass throughput rate; (■) spinning temperature; (▲) take-up velocity.

This work was supported by the Research Fund for Advanced Materials (in 1996) of the Ministry of Education, Republic of Korea.

REFERENCES

1. M. Matsui, *Sen-I Kikai Gakkaishi,* **34**(7), 319 (1981).
2. T. Takeda, *Sen-I Gakkaishi,* **48**(7), 405 (1992).
3. T. Nakajima, K. Kajiwara, and J. E. McIntyre, *Advanced Fiber Spinning Technology,* Woodhead, Cambridge, 1994.
4. B. D. Freeman, M. M. Denn, R. Keunings, G. E. Molau, and T. Ramos, *J. Polym. Eng.,* **6,** 171 (1986).
5. I. Cabasso, *Hollow Fiber Membranes in Encyclopedia of Chemical Technology,* **12,** 492 (1981).
6. J. Scott, *Hollow Fibers: Manufacture and Applications,* Noyes Data Corporation, Park Ridge, NJ, 1981.
7. A. Ziabicki, *Kollid Z.,* **171,** 51 (1960).
8. S. Kase and T. Matsuo, *J. Appl. Polym. Sci.,* **3,** 2541 (1965).
9. S. Kase and T. Matsuo, *J. Appl. Polym. Sci.,* **11,** 251 (1967).
10. D. K. Gagon and M. M. Denn, *Polym. Eng. Sci.,* **21,** 844 (1981).
11. H. H. George, *Polym. Eng. Sci.,* **22,** 292 (1982).
12. A. Dutta and V. M. Nadkarni, *Tex. Res. J.,* **54,** 35 (1984).
13. T. M. Getmanyuk, A. L. Yarin, I. M. Velikanova, L. P. Braverman, and R. G. Papernik, *Fibre Chem.,* **21,** 235 (1990).
14. R. E. Nickell, R. I. Tanner, and B. Caswell, *J. Fluid Mech.,* **65,** 189 (1974).
15. E. Mitsoulis and F. L. Heng, *AIChE J.,* **32,** 497 (1986).
16. M. J. Crochet and R. Keunings, *J. Non-Newtonian Fluid Mech.,* **7,** 199 (1980).
17. J. Cao, T. Kikutani, A. Takaku, and J. Shimizu, *J. Appl. Polym. Sci.,* **37,** 2683 (1989).
18. A. Ziabicki, *Fundamentals of Fibre Formation,* Wiley-Interscience, London, 1976.
19. C. D. Han, *J. Appl. Polym. Sci.,* **15,** 1091 (1976).
20. N. Orbey and J. M. Dealy, *Polym. Eng. Sci.,* **24,** 511 (1984).
21. A. Garcia-Rejon and J. M. Dealy, *Polym. Eng. Sci.,* **22,** 158 (1982).
22. A. M. Henderson and A. Rudin, *J. Appl. Polym. Sci.,* **31,** 353 (1986).